

Strong covalency-induced unusual defect physics in photovoltaic perovskite variant Cs_2SnI_6

Zewen Xiao,^{1,2} Hideo Hosono,^{1,2} and Toshio Kamiya^{1,2,a)}

¹ *Materials and Structures Laboratory, Tokyo Institute of Technology, 4259 Nagatsuta, Midori-ku, Yokohama 226-8503, Japan*

² *Materials Research Center for Element Strategy, Tokyo Institute of Technology, 4259 Nagatsuta, Midori-ku, Yokohama 226-8503, Japan*

ABSTRACT: Cs_2SnI_6 is an air-stable & non-toxic variant of perovskite-type photovoltaic materials. In this letter, stability of intrinsic defects in Cs_2SnI_6 was examined by density functional theory calculations. We found that iodine vacancy and tin interstitial are the dominant defects, mainly responsible for the intrinsic *n*-type conductivity in Cs_2SnI_6 . However, the transition levels of the dominant defects are deep, which makes it difficult to achieve high-density *n*-type doping. Tin vacancy is expected for *p*-type doping, but it has a very high formation energy > 3.6 eV because of the strong Sn–I covalent bonds and can hardly be generated. Instead, cesium vacancy is formed at an extremely Cs-poor condition and explains already-reported *p*-type conductivity by SnI_2 doping.

^{a)} Email: kamiya.t.aa@m.titech.ac.jp.

Halide perovskites have recently been introduced as the “game-changer” materials in the novel solid-state solar cells.¹⁻⁴ These compounds have the general chemical formula ABX_3 ($A = Cs, CH_3NH_3,$ or $CH_2NH=CH$; $B = Pb$ or Sn ; $X = I, Br$ or Cl), where the A cations sit in the cubic or pseudo-cubic network of corner-sharing BX_6 octahedra. Regardless of unprecedented high efficiency (up to 20.1%) achieved in lead halide perovskite ($APbX_3$) solar cells, the toxicity of lead is an obstacle to overcome. To tackle the toxicity issue, tin (Sn)-derivatives have been examined to replace the Pb-based perovskites.⁵⁻⁸ However, such Sn-derivatives are extremely sensitive to the ambient atmosphere (oxygen, moisture, etc.).⁶⁻¹⁰ It has been suggested that the instability would originate from the low formation energy of Sn vacancy (V_{Sn}).¹¹ Therefore, a group of perovskite variant A_2SnX_6 has been developed, in which the Sn atom is strongly covalent-bonded and stabilized due to the shrinkage of the crystal lattice.¹¹ As a typical example in the A_2SnX_6 group, Cs_2SnI_6 has been reported to be an air-stable material, and its solar cells exhibit promising power conversion efficiencies (PCEs) up to 7.8%.¹² It has been reported that pristine Cs_2SnI_6 (formed at 475K) possesses an electron mobility of $310 \text{ cm}^2 \text{ V}^{-1}\text{s}^{-1}$ and doping with SnI_2 yields a *p*-type Cs_2SnI_6 , both of which have similar low carrier concentrations of $\sim 1 \times 10^{14} \text{ cm}^{-3}$.¹² In contrast to the above observation, interestingly, Zhang et al.¹³ observed very high resistivity instead in room temperature processed Cs_2SnI_6 . Further, our previous density functional theory (DFT) study indicates the oxidation state of Sn in Cs_2SnI_6 is close to +2 and not +4.¹¹ However, the typical Sn^{2+} -based compounds, including SnO ,¹⁴ SnS ,¹⁵ and $CsSnI_3$,¹⁶ in general, intrinsically exhibit good *p*-type conductivity because V_{Sn} in these compounds can easily be formed and act as shallow

acceptors to produce good *p*-type conductivities. However, undoped Cs₂SnI₆, which may be classified as a Sn²⁺-based compound based on the real charge calculated by our previous DFT calculations,¹¹ intrinsically exhibits high resistivity as described above. To clarify the origin of such unusual conductivity in Cs₂SnI₆, a systematic study on the defects in such an air-stable perovskite variant is important. Also, understanding of the electronic properties and defect kinetics of Cs₂SnI₆ would provide theoretical guidance for designing photovoltaic and other applications.

Here, we studied the formation enthalpy (ΔH) of intrinsic defects in Cs₂SnI₆ by DFT calculations. It was clarified that I vacancy (V_I) and Sn interstitial (Sn_i) are mainly responsible for the intrinsic *n*-type conductivity in Cs₂SnI₆. V_{Sn}, usually a dominant *p*-type defect, is hardly formed in Cs₂SnI₆ because of its high ΔH which is caused by the strong Sn–I covalent bonds in the isolated [SnI₆]²⁻ cluster. It would be unlikely to achieve intrinsic *p*-type conductivity in pure Cs₂SnI₆ due to the absence of an effective acceptor with sufficiently low ΔH and a shallow transition level.

Defect calculations were performed in the framework of DFT using the projector-augmented wave (PAW) method as implemented in the Vienna Ab initio Simulation Package (VASP 5.3).¹⁷ Cs (5s)(5p)(6s), Sn (5s)(5p), and I (5s)(5p) orbitals are treated as valence states in the PAW potentials. The cutoff energy for the basis set was set to 275.4 eV. A 72-atoms supercell (2 × 2 × 2 primitive cells) was used to model the intrinsic defects. Atomic positions were relaxed until all the forces on the atoms were less than 0.05 eV/Å, employing a Γ -centered 3 × 3 × 3 *k*-mesh and the Perdew–Burke–Ernzerhof (PBE96)¹⁸ generalized gradient approximation (GGA) functionals. The total energies were

calculated by Γ point-only calculation with the Heyd–Scuseria–Ernzerhof (HSE06)¹⁹ hybrid functional with 34% of exact nonlocal exact exchange, which was confirmed to reproduce the experimental band gap of 1.26 eV as reported in Ref. 11.

ΔH of a defect (D) in a charge state q was calculated through the following equation²⁰

$$\Delta H_{D,q}(E_F, \mu) = E_{D,q} - E_H + \sum n_\alpha \mu_\alpha + q(E_F + E_V + \Delta V), \quad (1)$$

where $E_{D,q}$ is the total energies of the supercell with the defect D in the charge state q , and E_H that of the perfect host supercell. n_α indicates the number of α atoms added ($n_\alpha > 0$) or removed ($n_\alpha < 0$), and μ_α is the chemical potential of an α atom with respect to that of an elemental phase (μ_α^{el}) by $\mu_\alpha = \mu_\alpha^{\text{el}} + \Delta\mu_\alpha$. E_F is the Fermi level relative to the valence band maximum (VBM, E_V), which was corrected by ΔV through electrostatic potential alignment.²⁰ For charged defects, the image charge correction was also applied to eliminate the supercell finite-size effects.²¹

μ_α varies depending on the experimental condition during growth or annealing. First, to stabilize the Cs_2SnI_6 phase, the following thermodynamic equation must be satisfied

$$2\Delta\mu_{\text{Cs}} + \Delta\mu_{\text{Sn}} + 6\Delta\mu_{\text{I}} = \Delta H(\text{Cs}_2\text{SnI}_6) = -10.49 \text{ eV}, \quad (2)$$

where $\Delta H(\text{Cs}_2\text{SnI}_6)$ is ΔH of Cs_2SnI_6 referred to the elemental Cs, Sn, and I. To avoid the coexistence of the Cs, the Sn, and the I elemental phases, the additional conditions, $\Delta\mu_{\text{Cs}} < 0$, $\Delta\mu_{\text{Sn}} < 0$, and $\Delta\mu_{\text{I}} < 0$, are required. To exclude the secondary phases CsI (cubic, space

group $Pm\bar{3}m$),²² SnI₂ (monoclinic, space group $C2/m$),²³ SnI₄ (cubic, space group $Pa\bar{3}$),²⁴ and CsSnI₃ (cubic, space group $Pm\bar{3}m$),⁸ the following constraints must be satisfied as well.

$$\Delta\mu_{\text{Cs}} + \Delta\mu_{\text{I}} < \Delta H(\text{CsI}) = -3.80 \text{ eV}, \quad (3)$$

$$\Delta\mu_{\text{Sn}} + 2\Delta\mu_{\text{I}} < \Delta H(\text{SnI}_2) = -1.69 \text{ eV}, \quad (4)$$

$$\Delta\mu_{\text{Sn}} + 4\Delta\mu_{\text{I}} < \Delta H(\text{SnI}_4) = -2.40 \text{ eV}, \quad (5)$$

$$\Delta\mu_{\text{Cs}} + \Delta\mu_{\text{Sn}} + 3\Delta\mu_{\text{I}} < \Delta H(\text{CsSnI}_3) = -5.77 \text{ eV}. \quad (6)$$

With all these equations satisfied, $\Delta\mu_{\text{Cs}}$ and $\Delta\mu_{\text{I}}$ (and, thus, $\Delta\mu_{\text{Sn}}$ determined from Eq 2) are limited to a narrow region as shown by the yellow region defined by the A–B–C–D points in Figure 1. The narrow shape indicates that the growth or annealing conditions should be carefully controlled to produce the single-phase Cs₂SnI₆, similar to the cases of CsSnI₃¹⁶ and MAPbI₃.²⁵

From the $\Delta H_{D,q}$, the defect transition level $\varepsilon(q/q')$ between two charge states q and q' is obtained as the E_{F} where $\Delta H_{D,q}(E_{\text{F}},q) = \Delta H_{D,q}(E_{\text{F}},q')$. The defect concentrations were calculated by the following equation²⁶

$$c_{D,q}(E_{\text{F}},\mu,T) = N_{D,q} \exp[\Delta S_{D,q}/k_{\text{B}} - \Delta H_{D,q}(E_{\text{F}},\mu)/k_{\text{B}}T_D], \quad (7)$$

where $N_{D,q}$ is the density of the defect sites, $\Delta S_{D,q}$ the formation entropy (typically, $(1-10)k_{\text{B}}$ ²⁶), k_{B} the Boltzmann constant, and T_D the growth or annealing temperature (i.e.,

the temperature where the defect density was determined). The equilibrium Fermi level ($E_{F,e}$) and carrier concentration at room temperature (i.e. measurement temperature) for given μ and T_D were determined using the calculated density of states (DOS) by solving semiconductor statistic equations self-consistently so as to satisfy the charge neutrality.²⁶

We have considered intrinsic point defects in Cs_2SnI_6 including three vacancies (V_{Cs} , V_{Sn} , V_{I}), three interstitials (Cs_i , Sn_i , I_i), two cation substitutions (Cs_{Sn} , Sn_{Cs}), and four antisites (Cs_{I} , Sn_{I} , I_{Cs} , I_{Sn}). Two representative chemical potential conditions in Figure 1 are considered here; ($\Delta\mu_{\text{Cs}}$, $\Delta\mu_{\text{I}}$) at B (I-rich) and D (I-poor) points. The calculated $\Delta H_{D,q}(E_{\text{F}},\mu)$ are plotted as a function of E_{F} in Figure 2. The calculated transition energy levels are plotted relative to the conduction band minimum (CBM) and valence band maximum (VBM) in Figure 3. Out of the twelve intrinsic defects, four have a sufficiently small ΔH (e.g., < 1.0 eV) to influence the electrical properties. Among them, V_{I} has the lowest ΔH (≤ 0.74 eV and ≤ 0.28 eV under I-rich and I-poor conditions, respectively) and acts as a deep donor with $\varepsilon(0/+1) = 0.74$ eV above VBM (i.e., 0.52 eV below the conduction band edge, CBM), which is mainly responsible for the poor n -type conductivity of Cs_2SnI_6 . It has been suggested that strong covalence generally leads to the deep vacancy level.^{25,27} The deep transition of V_{I} in Cs_2SnI_6 can be attributed to the strong Sn–I bonds (2.41 eV/bond) in the $[\text{SnI}_6]^{2-}$ cluster.¹¹ Under the I-poor condition, Sn_i has a small ΔH (≤ 1.18 eV) and a shallower transition $\varepsilon(0/+1)$ at 0.11 eV below the CBM. Therefore, Sn_i as well as V_{I} are also dominant donors for n -type conductivity. Only Sn_{I} is a shallow donor in Cs_2SnI_6 with the $\varepsilon(0/+2)$ above the CBM, as seen in Figure 3. However, because of its relatively high ΔH , Sn_{I} has limited contribution to the n -type conductivity even under the I-poor condition. On

the other hand, under the I-rich condition, V_{Cs} has a low ΔH (≤ 1.37 eV) and can act as an acceptor at E_F above 0.51 eV from the VBM. However, the holes produced by the V_{Cs} hardly compensate the electrons released by V_I because of the deep $\epsilon(0/+1)$ at 0.51 eV for V_{Cs} . Cs_I is of a low ΔH but stabilized in the neutral charge state at high E_F ; therefore, it does not contribute to the n -type conductivity.

The defects with high ΔH are displayed by dashed lines in Figure 2. It should be noted that V_{Sn} in Cs_2SnI_6 has high ΔH values under all the chemical potentials and is 3.63 eV even under the Sn-poor condition (A point), as seen in Table 1. This is unusual compared with other typical Sn^{2+} -based semiconductors such as SnO ,¹⁴ SnS ,¹⁵ and $CsSnI_3$,¹⁶ in which the ΔH values of V_{Sn} (at the VBM) are usually very small under the Sn-poor condition (i.e., 1.3 eV for SnO ,¹⁴ 0.8 eV for SnS ,¹⁵ and 0.3 eV for $CsSnI_3$ ¹⁶). The unusually high ΔH of V_{Sn} in Cs_2SnI_6 is attributed to the strong Sn–I bonds. Besides, for the same reason, Cs_{Sn} and I_{Sn} also have high ΔH values. We have proposed that the +2 valence state of Sn in Cs_2SnI_6 is stabilized by the strong covalent Sn–I bonds.¹¹ Here, the high ΔH of the above Sn-related defects further support the stabilized +2 valence state of Sn in Cs_2SnI_6 .

The transition levels of the dominant defects are important for performance of solar cells because $\epsilon(q/q')$ in the band gap indicates that they work as an electron trap, hole trap and/or a recombination center and deteriorate the device performance. The dominant defects V_{Pb} in $MAPbI_3$ ²⁵ and V_{Sn} in $CsSnI_3$ ¹⁶ have transitions deeper than their VBMs and are inert. Also in $CuInSe_2$, the dominant defect V_{Cu} has a transition level only 0.03 eV above the VBM.²⁸ The very shallow V_{Cu} results in p -type conductivity but does not deteriorate the photovoltaic performance. In Cs_2SnI_6 , all the dominant defects (Cs_i , Sn_i , V_I ,

V_{CS} as shown by the solid lines in Figure 2) have $\varepsilon(q/q')$ in the band gap, as seen in Figure 3, which would more or less hinder its high performance as a photovoltaic semiconductor. Besides, because of the lack of p -type defects with shallow transition levels, it would be difficult to achieve intrinsic p -type conductivity in Cs_2SnI_6 .

Figure 4 shows the calculated and measured electron concentrations (n) as a function of T_D . The theoretical n is maximal under the I-poor (the D point) condition and minimal under the I-rich (the B point) condition. Under the I-poor condition (the blue lines in Figure 4), n is independent of T_D and of the order of 10^{14} cm^{-3} , because the ΔH of the donor defects V_I and Sn_i are low enough so that their densities are saturated. On the other hand, the limited n values are attributed to the relatively small effective conduction band density of state N_C (calculated to be $1.89 \times 10^{17} \text{ cm}^{-3}$ from DOS) and the deep $\varepsilon(0/+1)$ of V_I and Sn_i . Consequently, the equilibrium E_F is $E_{F,e} = 1.07 \text{ eV}$.

Under the I-rich condition (the red lines), for Cs_2SnI_6 grown at RT, i.e., $T_D = 300 \text{ K}$, the predicted n is of the order of $10^{10} - 10^{12} \text{ cm}^{-3}$, which is very low and difficult to be measured by usual Hall measurements. The n can be increased to the order of 10^{13} cm^{-3} by raising T_D to $>500 \text{ K}$.

These theoretical results seem explain the experimental results reported to date; i.e., the Cs_2SnI_6 thin films fabricated at RT have high resistivity and their the carrier density and type were not determined;¹³ while, the polycrystalline pellet of Cs_2SnI_6 synthesized at 473.15 K exhibited intrinsic n -type conductivity with n of the order of 10^{14} cm^{-3} .¹²

It should be noted that the above results are calculated for pure Cs_2SnI_6 phase, in which intrinsic p -type conductivity is unlikely to be achieved by controlling the growth or

annealing conditions because there are no effective intrinsic acceptors. On the other hand, there have been reports on carrier doping in Cs_2SnI_6 . For example, *p*-type conductivity has been reported in Cs_2SnI_6 by doping SnI_2 secondary phase.

Here, we like to discuss a possible origin of the carrier doping. We saw that the ($\Delta\mu_{\text{Cs}}$, $\Delta\mu_{\text{I}}$) chemical potential region for single-phase Cs_2SnI_6 (the yellow region in Figure 1) is fairly narrow; therefore, it is not easy to obtain single-phase Cs_2SnI_6 , and secondary phases may be formed once the chemical potential point is unintentionally moved out from the yellow region. The coexistence of secondary phases might significantly change the chemical potentials and influence the electrical properties of Cs_2SnI_6 . As we have reported that the real valence state of Sn in Cs_2SnI_6 is +2 and the same as that in SnI_2 ; therefore, the reported *p*-type conductivity cannot be explained by the conventional aliovalent atomic doping concept (i.e., substituting Sn^{4+} by Sn^{2+}). Instead, it would be explained by considering the fact that the extra addition of SnI_2 might provide a strong Cs-poor condition, which favors the formation of V_{Cs} to produce the *p*-type conductivity. For example, if the chemical potential point moves from the B point ($\Delta\mu_{\text{Cs}} = -4.04$ eV, $\Delta\mu_{\text{I}} = 0$ eV) to the X point (the dashed magenta line in Figure 1) ($\Delta\mu_{\text{Cs}} = -4.40$ eV, $\Delta\mu_{\text{I}} = 0$ eV) which is located at the boundary with the SnI_2 phase, the ΔH of V_{Cs} is reduced by 0.36 eV. Further, if the chemical potential is moved to the Y point ($\Delta\mu_{\text{Cs}} = -4.80$ eV, $\Delta\mu_{\text{I}} = 0.20$ eV), the ΔH of V_{Cs} is reduced by 0.76 eV while the ΔH of V_{I} is increased by 0.20 eV. As a result, the ΔH of neutral V_{Cs} (0.61 eV) becomes lower than that of neutral V_{I} (0.94 eV), which provides a weak *p*-type conductivity (for example, a hole density (*p*) of $1.0 \times 10^{11} \text{ cm}^{-3}$ is obtained when $T_{\text{D}} = 300\text{K}$ and $\Delta S_{D,q} = 5k_{\text{B}}$).

In summary, we have investigated the formation energies of intrinsic defects in Cs₂SnI₆ perovskite variant. The dominant defects are *n*-type V_I and Sn_i. However, their ε(0/+1) transitions are not shallow, for which the resulting *n* is limited to the order of 10¹⁴ cm⁻³. Unlike other Sn²⁺-based *p*-type semiconductor such as SnO, SnS and CsSnI₃, the V_{Sn} in Cs₂SnI₆ has a very high Δ*H* > 3.6 eV and can hardly be formed, primarily because of the strong Sn–I covalent bonds in the functional group-like [SnI₆]²⁻ cluster. Our results suggest that it is unlikely to achieve intrinsic *p*-type conductivity because of the lack of effective *p*-type defects, but possible if a secondary phase such as SnI₂ coexists. These results explain the reported experimental results and provide a clue to better understanding the unusual defect physics in *p*-block metal-based compounds.

This work was conducted under Tokodai Institute for Element Strategy (TIES) funded by MEXT Elements Strategy Initiative to Form Core Research Center. We would like to thank Mr. Yuanyuan Zhou and Prof. Nitin P. Padture at Brown University for valuable discussion.

¹A. Kojima, K. Teshima, Y. Shirai, T. Miyasaka, *J. Am. Chem. Soc.* **131**, 6050–6051 (2009).

²D. Shi, V. Adinolfi, R. Comin, M. Yuan, E. Alarousu, A. Buin, Y. Chen, S. Hoogland, A. Rothenberger, K. Katsiev, Y. Losovyj, X. Zhang, P. A. Dowben, O. F. Mohammed, E. H. Sargent, and O. M. Bakr, *Science* **347**, 519–522 (2015).

³N. J. Jeon, J. H. Hoh, Y. C. Kim, K. S. Yang, S. Ryu, and S. I. Seok, *Nat. Mater.* **13**,

897–903 (2014).

⁴N. J. Jeon, J. H. Noh, W. S. Yang, Y. C. Kim, S. Ryu, J. Seo, and S. I. Seok, *Nature* **517**, 476–480 (2015).

⁵F. Hao, C. C. Stoumpos, D. H. Cao, R. P. H. Chang, and M. G. Kanatzidis, *Nat. Photon.* **8**, 489–494 (2014).

⁶N. K. Noel, S. D. Stranks, A. Abate, C. Wehrenfennig, S. Guarnera, A.-A. Haghighirad, A. Sadhanala, G. E. Eperon, S. K. Pathak, M. B. Johnson, A. Petrozza, L. M. Herz, H. J. Snaith, *Energy Environ. Sci.* **7**, 3061–3068 (2014).

⁷I. Chung, B. Lee, J. He, R. P. H. Chang, and M. G. Kanatzidis, *Nature* **485**, 486–489. (2012).

⁸I. Chung, J. -H. Song, J. Im, J. Androulakis, C. D. Malliakas, H. Li, A. J. Freeman, J. T. Kenney, and M. G. Kanatzidis, *J. Am. Chem. Soc.* **34**, 8579–8587 (2012).

⁹Z. Chen, J. J. Wang, Y. Ren, C. Yu, and K. Shum, *Appl. Phys. Lett.* **101**, 093901 (2012).

¹⁰Y. Zhou, H. F. Garces, B. S. Senturk, A. L. Ortiz, and N. P. Padture, *Mater. Lett.* **110**, 127–129 (2013).

¹¹Z. Xiao, H. Lei, X. Zhang, Y. Zhou, H. Hosono, and T. Kamiya, *Electronic structure, valence state of Sn and chemical stability of photovoltaic perovskite variant Cs₂SnI₆*, submitted.

¹²B. Lee, C. C. Stoumpos, N. Zhou, F. Hao, C. Malliakas, C. -Y. Yeh, T. J. Marks, M. G. Kanatzidis, and R. P. H. Chang, *J. Am. Chem. Soc.* **136**, 15379–15385 (2014).

¹³J. Zhang, C. Yu, L. Wang, Y. Li, Y. Ren, and K. Shum, *Sci. Rep.* **4**, 6954 (2014).

¹⁴A. Togo, F. Oba, and I. Tanaka, *Phys. Rev. B* **74**, 195128 (2006).

- ¹⁵J. Vidal, S. Lany, M. d'Avezac, A. Zunger, A. Zakutyyev, J. Francis, and J. Tate, *Appl. Phys. Lett.* **100**, 032104 (2012).
- ¹⁶P. Xu, S. Chen, H. -J. Xiang, X. -G. Gong, and S. -H. Wei, *Chem. Mater.* **26**, 6068–6072 (2014).
- ¹⁷G. Kresse and J. Furthmüller, *Phys. Rev. B* **54**, 11169–11186 (1996).
- ¹⁸J. P. Perdew, K. Burke, and M. Ernzerhof, *Phys. Rev. Lett.* **77**, 3865–3868 (1996).
- ¹⁹J. Heyd, G. E. Scuseria, and M. Ernzerhof, *J. Chem. Phys.* **124**, 219906 (2006).
- ²⁰C. G. Van de Walle and J. Neugebauer, *Appl. Phys. Rev.* **95**, 3851–3879 (2004).
- ²¹S. Lany and A. Zunger, *Phys. Rev. B* **78**, 235104 (2008).
- ²²A. Smakula and J. Kalnajs, *Phys. Rev.* **99**, 1737–1743 (1955).
- ²³R. A. Howie, W. Moser, and I. C. Trevena, *Acta. Cryst.* **B28**, 2965–2971 (1972).
- ²⁴R. G. Dickinson, *J. Am. Chem. Soc.* **45**, 958–962 (1923).
- ²⁵W. -J. Yin, T. Shi, and Y. Yan, *Appl. Phys. Lett.* **104**, 063903 (2014).
- ²⁶D. B. Laks, C. G. Van de Walle, G. F. Neumark, P. E. Blöchl, and S. T. Pantelides, *Phys. Rev. B* **45**, 10965–10978 (1992).
- ²⁷W. -J. Yin, S. -H. Wei, M. M. Al-Jassim, and Y. Yan, *Appl. Phys. Lett.* **99**, 142109 (2011).
- ²⁸S. B. Zhang, S. -H. Wei, A. Zunger, and H. Katayama-Yoshida, *Phys. Rev. B* **57**, 9642–9656 (1998).

Tables and captions:

Table I. Formation enthalpies (unit: eV) of twelve natural intrinsic defects in Cs_2SnI_6 at the chemical potential points A, B, C, and D shown in Figure 1b.

	V_{Cs}	V_{Sn}	V_{I}	Cs_i	Sn_i	I_i	Cs_{Sn}	Sn_{Cs}	Cs_{I}	Sn_{I}	I_{Cs}	I_{Sn}
A	1.61	3.63	0.74	2.86	2.77	2.54	3.74	3.50	1.57	5.47	2.62	1.74
B	1.37	4.11	0.74	3.10	2.28	2.54	4.46	2.78	1.81	4.98	2.38	2.23
C	1.71	5.47	0.40	2.76	0.93	2.88	5.48	1.76	1.14	3.29	3.06	3.92
D	2.07	5.47	0.28	2.40	0.93	3.00	5.12	2.12	0.65	3.17	3.54	4.04

Figure captions:

FIG. 1. ($\Delta\mu_{\text{Cs}}$, $\Delta\mu_{\text{I}}$) chemical potential – phase map. The yellow region A–B–C–D shows the region where Cs_2SnI_6 is stabilized against possible competitive phases including Cs, Sn, I, CsI, SnI_2 , SnI_4 , and CsSnI_3 .

FIG. 2. Calculated ΔH of intrinsic defects in Cs_2SnI_6 as a function of E_{F} at the chemical potential points in Figure 1, (a) B (I-rich) and (b) D (I-poor). Defects with high ΔH values are shown by dashed lines.

FIG. 3. Calculated transition energy levels $\varepsilon(q/q')$ for intrinsic defects in Cs_2SnI_6 . Donor and acceptor defect levels are denoted by red and blue bars, respectively. The solid and open circles at the levels show the number of electrons and holes that can be released during the transition of the defect charge state.

FIG. 4. Calculated electron density (n) at RT as a function of the growth or annealing temperature (T_{D}) at A (black), B (red), C (green), and D (blue) chemical potential points by assuming $\Delta S_{D,q} = k_{\text{B}}$ (dash), and $\Delta S_{D,q} = 10k_{\text{B}}$ (solid). The experimental data from Ref. 11 are shown by symbols for comparison.

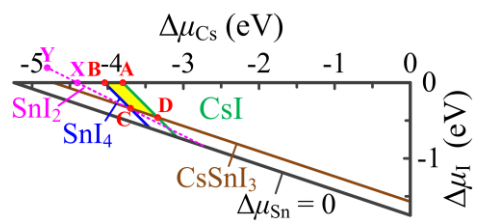


FIG. 1. Xiao *et al*

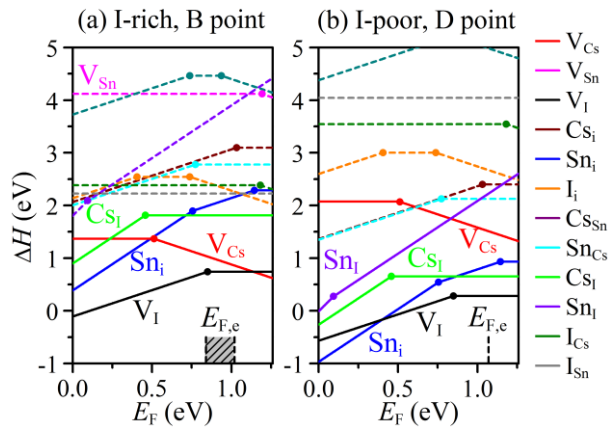


FIG. 2. Xiao *et al*

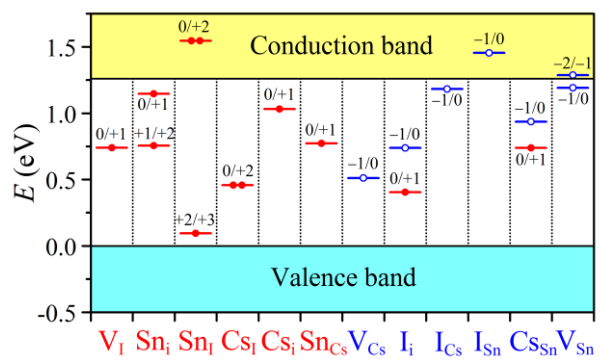


FIG. 3. Xiao et al

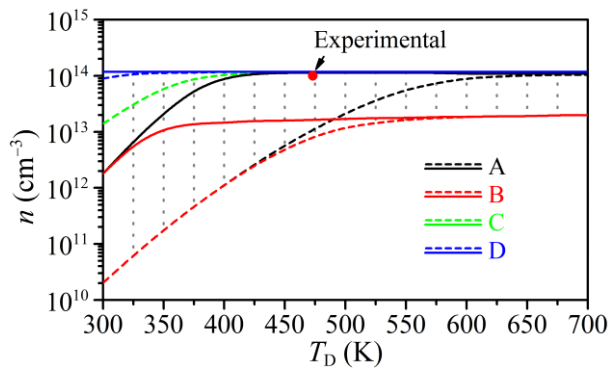


FIG. 4. Xiao *et al*